Optical cavity modes of a single crystalline zinc oxide microsphere

Rakesh Singh Moirangthem,[1,2] Pi-Ju Cheng,[1,3] Paul Ching-Hang Chien,[1,3] Buu Trong Huynh Ngo,[1,4,5] Shu-Wei Chang,[1,3,6] Chung-Hao Tien,[3] and Yia-Chung Chang[1,3,*]

[1]Research Center for Applied Sciences, Academia Sinica, Taipei, 11529, Taiwan
[2]Max-Planck-Institut fur Eisenforschung, Max-Planck-Strasse 1 Dusseldorf, 40237, Germany
[3]Department of Photonics, National Chiao Tung University, Hsinchu 30010, Taiwan
[4]Nano Science and Technology Program, TIGP, Academia Sinica, Taipei 11529, Taiwan
[5]Department of Engineering and System Science, National Tsing Hua University, Hsinchu 30010, Taiwan
[6]swchang@sinica.edu.tw
**yiachang@gate.sinica.edu.tw*

Abstract: A detailed study on the optical cavity modes of zinc oxide microspheres under the optical excitation is presented. The zinc oxide microspheres with diameters ranging from 1.5 to 3.0 μm are prepared using hydrothermal growth technique. The photoluminescence measurement of a single microsphere shows prominent resonances of whispering gallery modes at room temperature. The experimentally observed whispering gallery modes in the photoluminescence spectrum are compared with theoretical calculations using analytical and finite element methods in order to clarify resonance properties of these modes. The comparison between theoretical analysis and experiment suggests that the dielectric constant of the ZnO microsphere is somewhat different from that for bulk ZnO. The sharp resonances of whispering gallery modes in zinc oxide microspheres cover the entire visible window. They may be utilized in realizations of optical resonators, light emitting devices, and lasers for future chip integrations with micro/nano optoelectronic circuits, and developments of optical biosensors.

OCIS codes: (140.4780) Optical resonators; (140.3945) Microcavities; (250.5230) Photoluminescence.

References and links

1. S. Xu and Z. L. Wang, "One-dimensional ZnO nanostructures: Solution growth and functional properties," Nano Res. **4**(11), 1013–1098 (2011).
2. Z. Fan and J. G. Lu, "Zinc oxide nanostructures: synthesis and properties," J. Nanosci. Nanotechnol. **5**(10), 1561–1573 (2005).
3. D. J. Rogers, F. H. Teherani, V. E. Sandana, and M. Razeghi, "ZnO thin films and nanostructures for emerging optoelectronic applications," Proc. SPIE **7605**, 76050K, 76050K-11 (2010).
4. A. B. Djurisic, X. Chen, Y. H. Leung, and A. M. C. Ng, "ZnO nanostructures: growth, properties and applications," J. Mater. Chem. **22**(14), 6526–6535 (2012).
5. X. L. Wu, S. J. Xiong, Z. Liu, J. Chen, J. C. Shen, T. H. Li, P. H. Wu, and P. K. Chu, "Green light stimulates terahertz emission from mesocrystal microspheres," Nat. Nanotechnol. **6**(2), 103–106 (2011).
6. X. W. Sun, J. Z. Huang, J. X. Wang, and Z. Xu, "A ZnO nanorod inorganic/organic heterostructure light-emitting diode emitting at 342 nm," Nano Lett. **8**(4), 1219–1223 (2008).
7. Y. S. Choi, J. W. Kang, D. K. Hwang, and S. J. Park, "Recent advances in ZnO-based light-emitting diodes," IEEE Trans. Eletron. Dev. **57**(1), 26–41 (2010).
8. M. H. Huang, S. Mao, H. Feick, H. Q. Yan, Y. Wu, H. Kind, E. Weber, R. Russo, and P. Yang, "Room-temperature ultraviolet nanowire nanolasers," Science **292**(5523), 1897–1899 (2001).
9. S. Chu, G. Wang, W. Zhou, Y. Lin, L. Chernyak, J. Zhao, J. Kong, L. Li, J. Ren, and J. Liu, "Electrically pumped waveguide lasing from ZnO nanowires," Nat. Nanotechnol. **6**(8), 506–510 (2011).
10. D. J. Gargas, M. E. Toimil-Molares, and P. Yang, "Imaging single ZnO vertical nanowire laser cavities using UV-laser scanning confocal microscopy," J. Am. Chem. Soc. **131**(6), 2125–2127 (2009).
11. M. Law, L. E. Greene, J. C. Johnson, R. Saykally, and P. Yang, "Nanowire dye-sensitized solar cells," Nat. Mater. **4**(6), 455–459 (2005).
12. H. M. Chen, C. K. Chen, C. C. Lin, R. S. Liu, H. Yang, W. S. Chang, K. H. Chen, T. S. Chan, J. F. Lee, and D. P. Tsai, "Multi-bandgap-sensitized ZnO nanorod photoelectrode arrays for water splitting: an X-ray absorption

#180785 - $15.00 USD Received 29 Nov 2012; revised 17 Jan 2013; accepted 22 Jan 2013; published 31 Jan 2013

spectroscopy approach for the electronic evolution under solar illumination," J. Phys. Chem. C **115**(44), 21971–21980 (2011).
13. H. R. Liu, G. X. Shao, J. F. Zhao, Z. X. Zhang, Y. Zhang, J. Liang, X. G. Liu, H. S. Jia, and B. S. Xu, "Worm-like Ag/ZnO core-shell heterostructural composites: fabrication, characterization, and Photocatalysis," J. Phys. Chem. C **116**(30), 16182–16190 (2012).
14. G. X. Zhu, Y. J. Liu, H. Xu, Y. Chen, X. P. Shen, and Z. Xu, "Photochemical deposition of Ag nanocrystals on hierarchical ZnO microspheres and their enhanced gas-sensing properties," CrystEngComm **14**(2), 719–725 (2011).
15. X. Lu, H. Zhang, Y. Ni, Q. Zhang, and J. Chen, "Porous nanosheet-based ZnO microspheres for the construction of direct electrochemical biosensors," Biosens. Bioelectron. **24**(1), 93–98 (2008).
16. B. Q. Cao, K. Sakai, D. Nakamura, I. A. Palani, H. B. Gong, H. Y. Xu, M. Higashihata, and T. Okada, "Stimulated optical emission from ZnO nanobelts grown with a simple carbothermal evaporation method," J. Phys. Chem. C **115**(5), 1702–1707 (2011).
17. N. P. Herring, K. AbouZeid, M. B. Mohamed, J. Pinsk, and M. S. El-Shall, "Formation mechanisms of gold-zinc oxide hexagonal nanopyramids by heterogeneous nucleation using microwave synthesis," Langmuir **27**(24), 15146–15154 (2011).
18. H. Tang, G. Meng, Q. Huang, Z. Zhang, Z. Huang, and C. Zhu, "Arrays of cone-shaped ZnO nanorods decorated with Ag nanoparticles as 3D surface-enhanced raman scattering substrates for rapid detection of trace polychlorinated biphenyls," Adv. Funct. Mater. **22**(1), 218–224 (2012).
19. Y. H. Tseng, M. H. Liu, Y. W. Kuo, P. Chen, C. T. Chen, Y. F. Chen, and C. Y. Mou, "Biomimetic ZnO plate twin-crystals periodical arrays," Chem. Commun. (Camb.) **48**(26), 3215–3217 (2012).
20. G. P. Zhu, C. X. Xu, J. Zhu, C. G. Lv, and Y. P. Cui, "Two-photon excited whispering-gallery mode ultraviolet laser from an individual ZnO microneedle," Appl. Phys. Lett. **94**(5), 051106 (2009).
21. H. Dong, Z. Chen, L. Sun, W. Xie, H. H. Tan, J. Lu, C. Jagadish, and X. Shen, "Single-crystalline hexagonal ZnO microtube optical resonator," J. Mater. Chem. **20**(26), 5510–5515 (2010).
22. N. Wang, X. Cao, Q. Wu, R. Zhang, L. Wang, P. Yin, and L. Guo, "Hexagonal ZnO bipyramids: synthesis, morphological evolution, and optical properties," J. Phys. Chem. C **113**(52), 21471–21476 (2009).
23. S. Cho, J. W. Jang, S. H. Lee, J. S. Lee, and K. H. Lee, "A method for modifying the crystalline nature and texture of ZnO nanostructure surfaces," Cryst. Growth Des. **11**(12), 5615–5620 (2011).
24. S. S. Lo and D. Huang, "Morphological variation and Raman spectroscopy of ZnO hollow microspheres prepared by a chemical colloidal process," Langmuir **26**(9), 6762–6766 (2010).
25. Q. Li, K. Gao, Z. Hu, W. Yu, N. Xu, J. Sun, and J. Wu, "Photoluminescence and lasing properties of catalyst-free ZnO nanorod arrays fabricated by pulsed laser deposition," J. Phys. Chem. C **116**(3), 2330–2335 (2012).
26. D. J. Gargas, H. Gao, H. Wang, and P. Yang, "High quantum efficiency of band-edge emission from ZnO nanowires," Nano Lett. **11**(9), 3792–3796 (2011).
27. D. Wang, H. W. Seo, C. C. Tin, M. J. Bozack, J. R. Williams, M. Park, and Y. Tzeng, "Lasing in whispering gallery mode in ZnO nanonails," J. Appl. Phys. **99**(9), 093112 (2006).
28. D. J. Gargas, M. C. Moore, A. Ni, S. W. Chang, Z. Zhang, S. L. Chuang, and P. Yang, "Whispering gallery mode lasing from zinc oxide hexagonal nanodisks," ACS Nano **4**(6), 3270–3276 (2010).
29. Y. H. Yang, Y. Zhang, N. W. Wang, C. X. Wang, B. J. Li, and G. W. Yang, "ZnO nanocone: application in fabrication of the smallest whispering gallery optical resonator," Nanoscale **3**(2), 592–597 (2011).
30. R. Chen, B. Ling, X. W. Sun, and H. D. Sun, "Room temperature excitonic whispering gallery mode lasing from high-quality hexagonal ZnO microdisks," Adv. Mater. (Deerfield Beach Fla.) **23**(19), 2199–2204 (2011).
31. M. Wang, Y. Zhou, Y. Zhang, E. J. Kim, S. H. Hahn, and S. G. Seong, "Near-infrared photoluminescence from ZnO," Appl. Phys. Lett. **100**(10), 101906 (2012).
32. C. Czekalla, T. Nobis, A. Rahm, B. Cao, J. Zúñiga-Pérez, C. Sturm, R. Schmidt-Grund, M. Lorenz, and M. Grundmann, "Whispering gallery modes in zinc oxide micro- and nanowires," Phys. Status Solidi B **247**(6), 1282–1293 (2010).
33. F. Vollmer, D. Braun, A. Libchaber, M. Khoshsima, I. Teraoka, and S. Arnold, "Protein detection by optical shift of a resonant microcavity," Appl. Phys. Lett. **80**(21), 4057 (2002).
34. S. Pang, R. E. Beckham, and K. E. Meissner, "Quantum dot-embedded microspheres for remote refractive index sensing," Appl. Phys. Lett. **92**(22), 221108 (2008).
35. S. W. Chang, "Full frequency-domain approach to reciprocal microlasers and nanolasers-perspective from Lorentz reciprocity," Opt. Express **19**(22), 21116–21134 (2011).
36. Y. G. Wang, S. W. Chang, C. C. Chen, C. H. Chiu, M. Y. Kuo, M. H. Shih, and H. C. Kuo, "Room temperature lasing with high group index in metal-coated GaN nanoring," Appl. Phys. Lett. **99**(25), 251111 (2011).
37. S. Cho, J. W. Jang, A. Jung, S. H. Lee, J. Lee, J. S. Lee, and K. H. Lee, "Formation of amorphous zinc citrate spheres and their conversion to crystalline ZnO nanostructures," Langmuir **27**(1), 371–378 (2011).
38. S. Spillane, "Fiber-coupled ultra-high-Q microresonators for nonlinear and quantum optics," Ph.D. thesis, California Inst. of Technol. (2004).
39. S. Schiller, "Asymptotic expansion of morphological resonance frequencies in Mie scattering," Appl. Opt. **32**(12), 2181–2185 (1993).
40. M. Bass, *Handbook of Optics* 2nd Ed., Vol. 2. (McGraw-Hill, United States of America, 1994).
41. A. Chiasera, Y. Dumeige, P. Féron, M. Ferrari, Y. Jestin, G. Nunzi Conti, S. Pelli, S. Soria, and G. C. Righini, "Spherical whispering-gallery-mode microresonators," Laser Photon. Rev. **4**(3), 457–482 (2010).
42. A. B. Matsko, A. A. Savchenkov, D. Strekalov, V. S. Ilchenko, and L. Maleki, "Review of application of whispering-gallery mode resonators in photonics and nonlinear optics," IPN Progress Report 42–162 (2005).

#180785 - $15.00 USD Received 29 Nov 2012; revised 17 Jan 2013; accepted 22 Jan 2013; published 31 Jan 2013

43. R. Cuscó, E. A. Lladó, J. Ibáñez, L. Artús, J. Jiménez, B. Wang, and M. J. Callahan, "Temperature dependence of Raman scattering in ZnO," Phys. Rev. B **75**(16), 165202 (2007).
44. K. Vanheusden, C. H. Seager, W. L. Warren, D. R. Tallant, and J. A. Voigt, "Correlation between photoluminescence and oxygen vacancies in ZnO phosphors," Appl. Phys. Lett. **68**(3), 403–405 (1996).
45. D. Li, Y. H. Leung, A. B. Djurisic, Z. T. Liu, M. H. Xie, S. L. Shi, S. J. Xu, and W. K. Chan, "Different origins of visible luminescence in ZnO nanostructures fabricated by the chemical and evaporation methods," Appl. Phys. Lett. **85**(9), 1601–1603 (2004).
46. R. Schmidt-Grund, N. Ashkenov, M. M. Schubert, W. Czakai, D. Faltermeier, G. Benndorf, H. Hochmuth, M. Lorenz, and M. Grundmann, "Temperature-dependence of the refractive index and the optical transitions at the fundamental band-gap of ZnO," AIP Conf. Proc. **893**, 271–272 (2007).
47. R. Schmidt-Grund, H. Hilmer, A. Hinkel, C. Sturm, B. Rheinlander, V. Gottschalch, M. Lange, J. Zuniga-Perez, and M. Grundmann, "Two-dimensional confined photonic wire resonators- strong light-matter coupling," Phys. Status Solidi B **247**(6), 1351–1364 (2010).
48. J. E. Heebner, T. C. Bond, and J. S. Kallman, "Generalized formulation for performance degradations due to bending and edge scattering loss in microdisk resonators," Opt. Express **15**(8), 4452–4473 (2007).

1. Introduction

Zinc oxide (ZnO), a wide bandgap (~3.37eV) semiconductor material, has been studied in both forms of thin films and micro/nano structures in the past decades for their potential applications in various fields because of its tunable optical and electronic properties [1–5]. This material has several superior characteristics in terms of large exciton binding energy (60 meV), cost effectiveness, and environmental friendliness to those of gallium nitride (GaN) and makes itself one of the most prospective materials for applications in optoelectronics, energy harvesting, photocatalyst, sensors, and biotechnology applications [6–15]. To produce high-quality ZnO micro/nanostructures such as belts, pyramids, cones, hexagonal pancakes, rods, plates, needles, tubes, and hollow spheres, several methods including carbothermal evaporation, microwave synthesis, electro-deposition process, hydrothermal process, vapor-phase transport method, oxidation-sublimation process, and solution route [16–24] can be utilized, depending on details of fabrications.

Small micro/nanostructures made of ZnO with a high crystalline quality do show unique characteristics in photon emissions and lasing. For example, ZnO micro/nanostructures with hexagonal cross sections can show distinct mode confinement routes such as those of Fabry-Perot (FP) modes and whispering gallery modes (WGMs) and can be utilized as compact resonators. Recently, these structures have drawn considerable interest in applications of optical resonators such as microcavity lasing due to their unique geometry, high crystallinity, and excellent optical properties [20, 21, 25–29]. However, there exists the potential optical loss at corners of hexagonal ZnO micro/nanostructures [30], and therefore, an isotropic structure like spheres may be a better candidate to achieve efficient light confinements for developments of micro/nano optical resonators and lasers. In a recent report [31], Wang *et al.* has shown photoluminescence (PL) properties of sheet-constructed ZnO microspheres with broad emission spectra in the near-infrared (IR) regime without clear resonance peaks. For the resonator performance, a smooth surface morphology of ZnO microspheres is crucial since a high quality factor and low lasing threshold of micro/nanocavities are only achievable without large scattering losses from rough surfaces. Only under such circumstances can whispering gallery modes, which are waves traveling around the circumference of the resonator due to the total internal reflection, exhibit sufficiently sharp resonances in various optical spectra.

The optical modes in ZnO microspheres are also sensitive to the local surrounding medium, and hence the mode strengths can act as remote transducing signal in response to local refractive index change upon adhesion of small molecules on spheres. With the radiative recombination in ZnO, the microsphere itself can also function as internal light sources [32]. Therefore, ZnO microspheres are promising for developments of WGM sensors in visible to near-IR spectral ranges in addition to the passive fiber couplers or microspheres doped with active centers [33, 34].

In this paper, we present the synthesis of ZnO microspheres with smooth surface and study the optical resonances of WGMs from single crystalline ZnO microsphere at room temperature using micro-PL (μ-PL) measurements. The observed optical resonances are compared with analytically estimated values and are further verified with a modified

#180785 - $15.00 USD Received 29 Nov 2012; revised 17 Jan 2013; accepted 22 Jan 2013; published 31 Jan 2013

eigenvalue formalism implemented with the axially symmetric finite-element method (FEM) [35, 36].

2. Experimental details

2.1. Synthesis of ZnO microspheres

ZnO microspheres were prepared through one-pot synthesis scheme using hydrothermal growth technique. Briefly, 50mM zinc nitrate hexahydrate [$Zn(NO_3)_2$•$6H_2O$] and hexamethylenetetramine [HMT] solution were prepared with the same molar ratio in ultrapure water and then mixed as well as stirred for 10 minutes until the chemicals were completely dissolved in the solvent. Next, the as-prepared 38mM trisodium citrate ($Na_3C_6H_5O_7$) in ultrapure water is mixed with the obtained solution with a volume ratio of 1:2 in a glass bottle. The mixed solution was put in a tightly closed glass bottle and placed inside the oven for 90 minutes at a fixed temperature of 90°C. White precipitations on the solution surface as well as sediments at the glass bottom were collected by centrifuging and later dispersed in the ultrapure water. After then, the prepared solution of ZnO microspheres was washed several times with water and then with ethanol to remove the contaminants. Finally, ZnO microspheres suspended in the ethanol solution were kept in the refrigerator until used. For the sample preparation, a drop of ethanol solution containing ZnO microspheres was placed on a pre-cleaned silicon substrate and kept inside the oven until dry. The sample was further annealed at 550 °C in the ambient atmosphere for 12 hours to improve crystallinity of the sample. The growth mechanism of the ZnO microspheres with similar technique has been reported [24, 37]. However, the growth mechanism of our ZnO microspheres is still unclear and is currently under investigation.

2.2. Characterization of samples

X-ray diffraction (XRD) studies on the annealed samples were performed using monochromatic CuKα_1 radiation. The morphology and structure studies of the ZnO microspheres were carried out using scanning electron microscope (SEM-Nano Nova) with an acceleration voltage of 10kV. Energy-dispersive microanalysis (EDX, Oxford instrument) was also performed on a single ZnO microsphere. The μ-PL and Raman measurements were carried out using a Horiba Jobin Yvon HR-800 UV setup with an excitation source of a He-Cd laser (325 nm line). For the μ-PL measurement, the excitation laser was focused onto single ZnO microspheres using a 40X UV objective (Thorlabs), and a similar objective was used to collect the scattered light from the microspheres into the detector. All of the PL data were recorded with liquid-nitrogen cooled silicon CCD detector through a grating of 2400 grooves mm^{-1} in the backscattering geometry. A 500μm confocal pinhole was used to obtain high resolution Raman spectra. All the optical measurements were performed at room temperature.

3. Theoretical analysis

Theoretical calculations are performed to estimate resonance wavelengths of WGMs in ZnO microspheres with various diameters. To simplify the problem, we first solve the transcendental equations of cavity modes in a dielectric sphere surrounded by an ambient environment [38], assuming that the WGMs of interest are not perturbed much due to the broken spherical symmetry from the Si substrate:

$$n^{1-2b}\frac{1}{zj_l(z)}\frac{\mathrm{d}[zj_l(z)]}{\mathrm{d}z}\bigg|_{z=nkR}-\frac{1}{zh_l^{(1)}(z)}\frac{\mathrm{d}[zh_l^{(1)}(z)]}{\mathrm{d}z}\bigg|_{z=kR}=0, \qquad (1)$$

where R and n are radius and refractive index of the dielectric sphere, respectively; $j_l(z)$ and $h_l^{(1)}(z)$ represent the spherical Bessel function and Hankel function of the first kind; l is the angular momentum mode number; k is the complex propagation constant which includes the effect of radiation loss in the ambient environment, and index b indicates whether the mode is

#180785 - $15.00 USD Received 29 Nov 2012; revised 17 Jan 2013; accepted 22 Jan 2013; published 31 Jan 2013

radially transverse magnetic (TM_r, $b = 1$) or radially transverse electric (TE_r, $b = 0$). The neglect of the subtract effect would be justified by the FEM calculations later.

We focus on the fundamental TE_r WGMs for each l (the least radially oscillatory modes confined near the equator for $b = 0$) since they are more likely to be longer-lived than other WGMs. The solutions to Eq. (1) for fundamental TE_r WGMs are denoted as $kR = x_l \equiv 2\pi R/\lambda_l$, where λ_l is a complex wavelength, and its real part $\mathrm{Re}[\lambda_l]$ represents the resonance wavelength. The characteristic values x_l are first estimated with the asymptotic expansion of Bessel function, which is close to the exact value if the mode number l is sufficiently large [39]. These estimations are then used as the initial guesses for iterations of Eq. (1) based on Newton-Raphson method. The dispersion is taken into account during iterations of x_l through $\mathrm{Re}[\lambda_l]$, from which the wavelength-dependent refractive index n of bulk ZnO is set [40]. The procedure leads to a series of resonance wavelengths $\mathrm{Re}[\lambda_l]$ as a function of mode number l.

These estimated wavelengths, nevertheless, cannot often match the experimental peak wavelengths well. Inaccurate mode spacings, missing resonances, and hence failures of one-to-one assignments between theory and experiment do occur. The uncertainty of material and structure parameters is expected to be the origin of mismatches. To make a sensible comparison, we need to (i) choose an indicator function to quantify the deviation, (ii) correctly assign mode numbers l to experimental resonances, and (iii) specify the origin of deviations. The diameter D of a microsphere is independent of WGM resonances and can be accurately obtained from SEM images. Therefore, we adopt this quantity as the indicator. Theoretically, the diameter is related to the characteristic value x_l as

$$D = 2R = \frac{x_l \lambda_l}{\pi} \approx \frac{\mathrm{Re}[x_l]\,\mathrm{Re}[\lambda_l]}{\pi}, \tag{2}$$

where we have used the fact that x_l and λ_l are dominated by their real parts. Thus, for a series of mode numbers $l \in [l_{\min}, l_{\min} + N_{\mathrm{Exp}} - 1]$, where $l_{\min}$ is the minimum for the assignment, and N_{Exp} is the number of resonances observed experimentally, we map the corresponding $\mathrm{Re}[x_l]$ to the consecutive experimental resonances labeled by index $l' \in [1, N_{\mathrm{Exp}}]$ one by one. The indicator function $D(l, l')$ defined as

$$D(l,l') \equiv \frac{\mathrm{Re}[x_l]\lambda_{\mathrm{Exp},l'}}{\pi}, \quad l' = l - l_{\min} + 1, \tag{3}$$

where $\lambda_{\mathrm{Exp},l'}$ is the experimental peak wavelength of the resonance l', shall reveal the deviation due to a particular mode assignment parameterized by $l_{\min}$ when compared with the diameters from SEM images. Ideally, the function $D(l,l')$ versus l should be a constant identical to the real diameters of microspheres.

With the indicator function in Eq. (3), we attempt to optimize the mode assignment under deviations of specific physical parameters. A simple origin that directly causes the imperfect assignment is the refractive index of ZnO. We do expect that the dispersive refractive index $n(\lambda)$ of the ZnO microsphere is different from that $n_{\mathrm{bulk}}(\lambda)$ of bulk [40]. To quantify this deviation, we utilize the group index $n_g(\lambda) \equiv \partial[n(\lambda)k]/\partial k$ for estimations. While the group index $n_{g,\mathrm{bulk}}(\lambda)$ of bulk ZnO is calculated from the frequency derivative of $n_{\mathrm{bulk}}(\lambda)$, the group index $n_g(\lambda)$ of the microsphere can be approximated with the simple WGM resonance condition $2\pi R = l\lambda_l/n(\lambda_l)$, which is valid at large l:

$$n_g(\lambda_l) \approx \frac{1}{R\Delta k_l} \equiv n_{g,\mathrm{Exp}}(\lambda_l), \tag{4}$$

where $\Delta k_l = k_{l+1} - k_l$ is obtained from experimental mode spacings of WGMs. The experimental measurement $n_{g,\mathrm{Exp}}(\lambda)$ is then curve-fitted with $n_{g,\mathrm{bulk}}(\lambda) + \Delta n$ by the least square-root method, where a frequency-independent constant Δn is introduced as the zeroth-order correction. The refractive index $n(\lambda)$ is accordingly corrected as $n_{\mathrm{bulk}}(\lambda) + \Delta n$. With this

#180785 - $15.00 USD Received 29 Nov 2012; revised 17 Jan 2013; accepted 22 Jan 2013; published 31 Jan 2013

modified index $n(\lambda)$, the indicator function $D(l,l')$ in Eq. (3) is utilized to find the proper mode assignment. As it will be shown later, a frequency-independent correction Δn is sufficient for satisfactory mode assignments in the visible range [41, 42]. Although a frequency-dependent correction to Δn can fit the experimental data better, it would involve using too many undetermined parameters, and is unnecessary at this stage.

4. Results and discussion

4.1. Morphology and crystallinity of the ZnO microspheres

Figure 1(a) shows SEM images of the annealed ZnO microspheres on the silicon (Si) substrate. The ZnO microspheres have very smooth surfaces and their diameters are in the range of 1.5 to 3.0 μm (see the inset images). The crystal structure of the ZnO microspheres is examined by the X-ray diffraction. Figure 1(b) displays the XRD pattern of the annealed ZnO microspheres, in which the strong and sharp peaks indicate the high purity and crystallinity of the microstructures. All of the diffraction peaks can be attributed to the hexagonal phase of

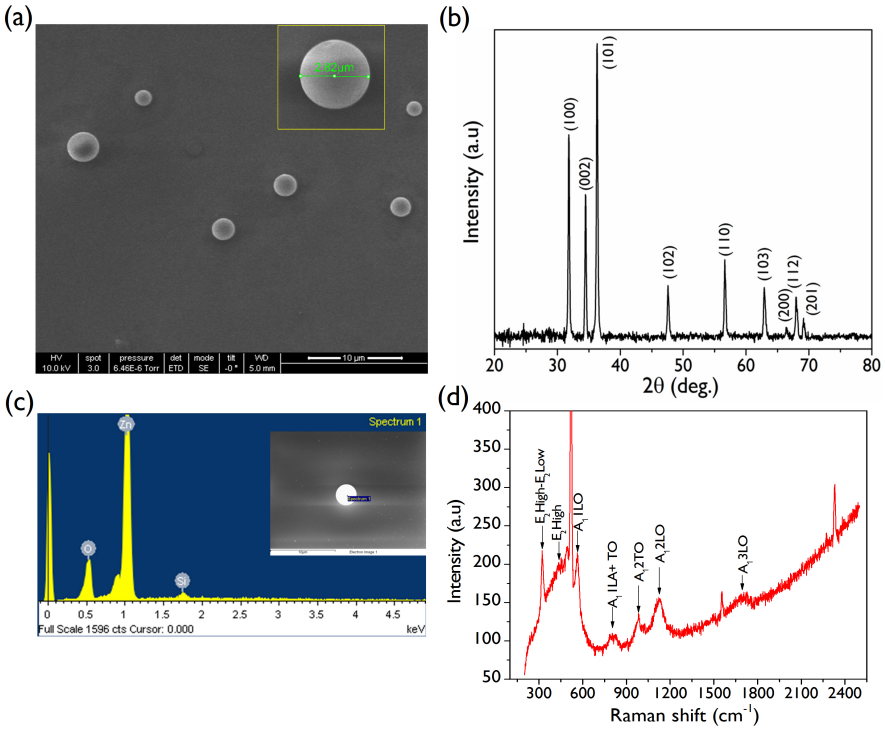

Fig. 1. (a) The SEM image of annealed ZnO microspheres on Si Substrate. (b) XRD pattern and (c) corresponding EDX spectrum from a single microsphere. (d) The room-temperature Raman scattering spectra of the as-prepared ZnO microspheres.

ZnO structure according to JCPDS card file no. 89-1397. The analysis of elemental compositions for these microspheres is performed with energy-dispersive X-ray (EDX) spectroscopy at an acceleration voltage of 10KV. Figure 1(c) shows the EDX spectrum from a single ZnO microsphere (see the inset). The data analysis indicates that typical microspheres are mostly composed of elements Zn and O. The signal of Si originates from the substrates due to the deep penetration of highly energetic electron beams through the microsphere.

The Raman spectroscopy is further employed to investigate the phase purity and crystallinity of wurtzite ZnO with the hexagonal structure. Figure 1(d) shows the Raman spectra of the as-prepared ZnO microspheres over the spectral range from 2000 to 2500 cm^{-1}

#180785 - $15.00 USD Received 29 Nov 2012; revised 17 Jan 2013; accepted 22 Jan 2013; published 31 Jan 2013

excited by the 325 nm line of a He-Cd laser. All the peaks in the spectra can be assigned to lattice vibrations of wurtzite ZnO [43]. The multiphonon process, E2 (high)-E2 (low) at 322 cm^{-1}, E2 (high) mode at 436 cm^{-1}, longitudinal optical mode with A1 symmetry, A11LO at 563 cm^{-1}, combination of longitudinal acoustic and transverse optical modes, A1(LA + TO) at 784 cm^{-1} and resonant peaks of multiple LO phonons up to the third order, are all clearly resolved in as-prepared ZnO microspheres. The other two peaks appearing at 1555 and 2331 cm^{-1} originate from the Si substrate. Before annealing, the Raman peak positions are slightly shifted toward the low energy side. In addition, the Raman intensity of the E2 (high) mode is often weaker than that after annealing, indicating that the as-prepared ZnO microspheres have a wurtzite lattice with poor crystallinity. After annealing at high temperature (550 °C), the crystallinity of the microspheres usually shows significant improvements, as reflected on the sharp peaks in the XRD pattern in Fig. 1(b).

4.2. Luminescence properties of isolated ZnO microspheres

The room temperature PL spectra of annealed ZnO microspheres taken at an excitation wavelength of 325 nm indicate clear resonances of WGMs over the entire visible and partial near-IR window. Experiments were performed with a normally incident laser beam toward

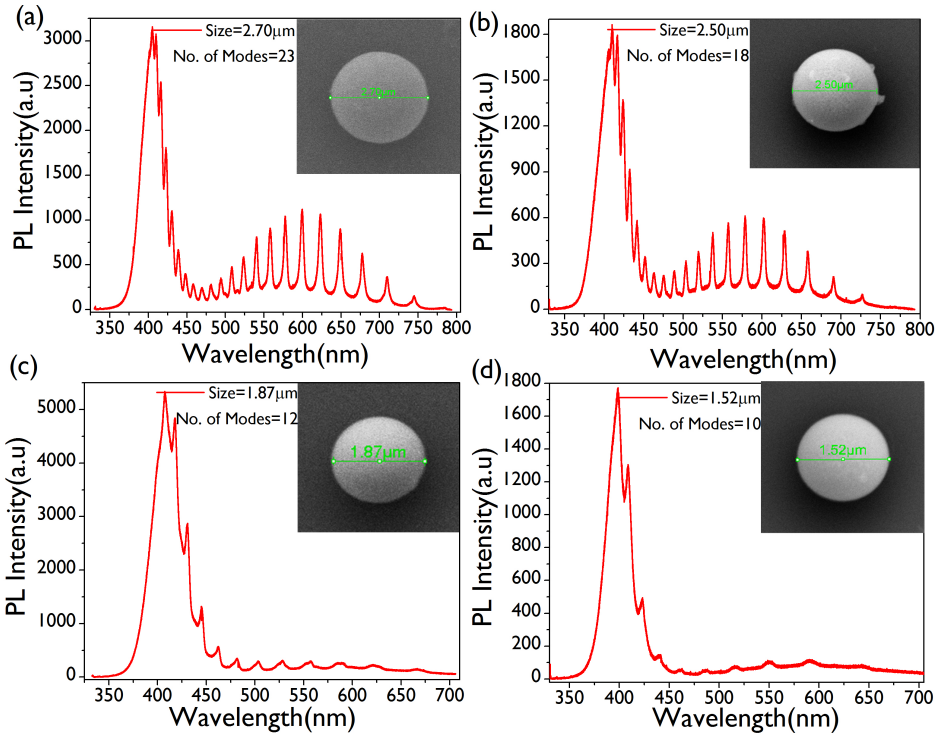

Fig. 2. PL spectra of a single ZnO microsphere placed on the Si substrate with diameters (a) 2.7 μm, (b) 2.5 μm, (c) 1.87 μm, and (d) 1.52 μm respectively.

#180785 - $15.00 USD Received 29 Nov 2012; revised 17 Jan 2013; accepted 22 Jan 2013; published 31 Jan 2013

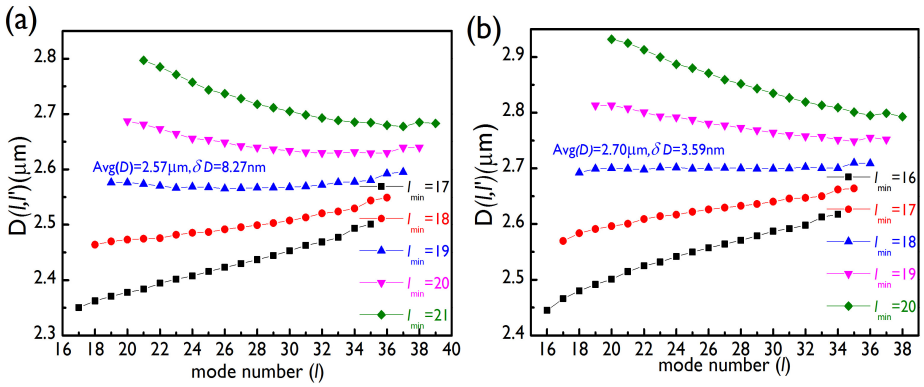

Fig. 3. The indicator function $D(l,l')$ versus mode number l for the ZnO microsphere with D = 2.7 μm. Function values under assignments parameterized by different l_{min} are shown for (a) $\Delta n = 0$ and (b) $\Delta n = -0.1852$.

the substrate, and the unpolarized emission spectra are taken. In the absence of the substrate effect, the TE_r and TM_r modes of the microsphere are degenerate.

Figure 2(a) shows the PL spectrum of a single ZnO microsphere with a diameter D = 2.7μm. The observed UV luminescence of these microspheres is attributed to room-temperature free-excitons near the band-edge of ZnO. However, the peak is shifted toward the low energy side from the typical value around 382 nm. This redshift could be due to excitons bound to some shallow impurities or intrinsic defects which arise during the growth. Further experimental and theoretical investigations are ongoing to clarify the origins of these shallow traps, which is not the current focus of study. In addition to the broad emission spectrum, the visible and near-IR luminescence is modulated by many sharp peaks of WGMs. The luminescence is generally believed to originate from different intrinsic deep-level defects in ZnO such as oxygen vacancy, zinc vacancy, and interstitial zinc [44, 45]. It is noted that the significant absorption above the band edge broadens the WGM resonances and makes them unobservable on the high-energy side of free-exciton emissions [32]. The number of modes and coupling strengths with the emitted photons also depend on diameters of microspheres. As observed from Fig. 2(b) to 2(d), the microsphere with a diameter D = 1.52 μm exhibits weak WGM resonances, and contrast ratios of these resonances improve gradually as the diameter of ZnO microsphere increases.

4.3. Theoretical comparison with experiments

Figures 3(a) shows the indicator $D(l,l')$ as a function of mode number l under different l_{min} for the microsphere with D = 2.7 μm, whose PL spectrum is shown in Fig. 2(a). The refractive index of bulk ZnO [40] is adopted in calculations of characteristic values x_l. In this case, the indicator function $D(l,l')$ is either off the diameter from the SEM image on average, or shows a significant variation with respect to the mode number l. For example, at l_{min} = 19, although $D(l,l')$ of different mode numbers l only give rise to a standard deviation of 8.27 nm, their average of 2.57 μm is quite different from the experimental value of 2.7 μm. Disagreements between $D(l,l')$ and the experimental values for all l_{min} indicate that some parameters used in theoretical estimations may be inadequate.

As addressed earlier, we speculate that the refractive index n of bulk ZnO which closely affects the spectral properties of modes is the origin of the discrepancy. The change in this quantity could be affected by several factors such as the annealing temperature and strain introduced to the crystal planes during the annealing process [46, 47]. Therefore, we add a frequency-independent correction Δn to the refractive index of bulk ZnO to account for the

#180785 - $15.00 USD Received 29 Nov 2012; revised 17 Jan 2013; accepted 22 Jan 2013; published 31 Jan 2013

Table 1. Comparisons between the experimental resonance wavelengths and those obtained from analytical estimations and FEM calculations for the fundamental TE$_r$-like WGMs of the microsphere with D = 2.7 μm.

Mode Index	20	21	22	23	24	25	26	27	28	29	30
$\lambda_{Exp.}$ (D = 2.7μm)	623	599	577	558	540	523	508	494	481	469	458
λ_{Ana} (TE$_r$) (D = 2.7μm)	622.9	599.1	577.5	557.7	539.7	523.1	507.9	493.9	481.0	469.1	458.1
λ_{FEM} (D = 2.7μm)	622.9	599.0	577.3	557.5	539.4	522.8	507.6	493.6	480.6	468.7	457.7

aforementioned effects on the refractive index. With Eq. (4) and related procedures, we set this correction to –0.1852 and show the corresponding indicator functions $D(l,l')$ under different l_{min} in Fig. 3(b). For l_{min} = 18, the function $D(l,l')$ is quite flat with a standard deviation of 3.59 nm. In addition, an average of 2.70 μm is consistent with that from the SEM image. The comparison indicates that the refractive index of ZnO microsphere is lower than that of bulk ZnO in the spectral range of the experiment. With the corrected refractive index of ZnO microsphere, the resonance wavelengths Re[λ_l] of the fundamental TE$_r$ WGMs at D = 2.7 μm are recalculated and listed in Table 1. We noticed very small differences in mode wavelengths (<0.4nm) between the analytic results and the FEM results, which are due to the substrate effect included in the FEM calculation.

The result now agrees well with the resonance peaks in experiment. In addition, the observation of sharp resonance peaks is indicative of decently clean and smooth surfaces of ZnO microspheres. Further increasing the optical pumping strength may turn the microspheres into a light emitting device above the band edge of ZnO. Similar analytical calculations were done for ZnO microsphere with D = 2.5 μm and corresponding results are shown in Fig. 4 and their values are listed in Table 2.

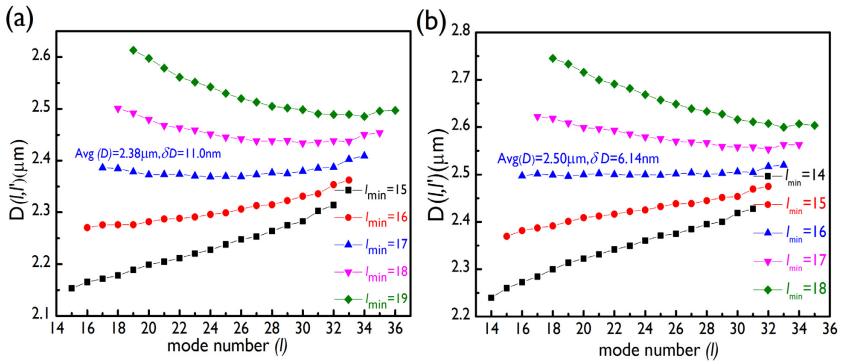

Fig. 4. The indicator function $D(l,l')$ versus mode number l for the ZnO microsphere with D = 2.5 μm. Function values under assignments parameterized by different l_{min} are shown for (a) Δn = 0 and (b) Δn = –0.1964.

Table 2. Comparisons between the experimental resonance wavelengths and those obtained from analytical estimations for the fundamental TEr-like WGMs of the microsphere with D = 2.5 μm.

Mode Index	18	19	20	21	22	23	24	25	26	27	28
$\lambda_{Exp.}$ (D = 2.5μm)	628	601	578	557	537	519	503	488	475	463	451
λ_{Ana} (TE$_r$) (D = 2.5μm)	628.3	601.9	578.1	556.5	537.0	519.2	503.0	488.3	474.7	462.3	451.0

#180785 - $15.00 USD Received 29 Nov 2012; revised 17 Jan 2013; accepted 22 Jan 2013; published 31 Jan 2013

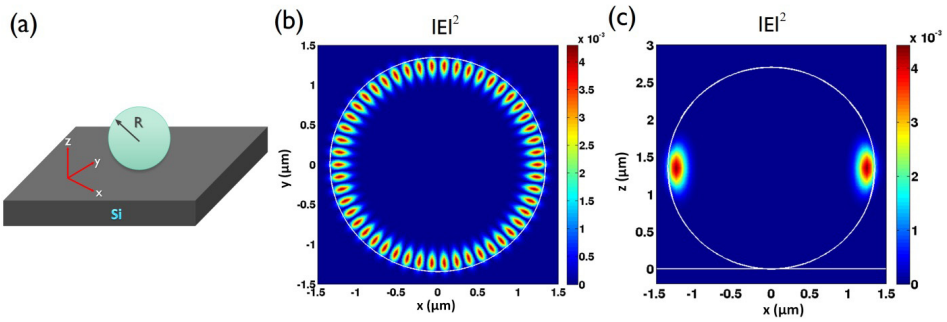

Fig. 5. (a) The schematic of a single ZnO microsphere on the Si substrate. (b) The top view of the WGM field profile near 522.83nm (l = 25) on the equatorial plane of the microsphere (z = R). (c) The side view on the vertical cross section (y = 0).

Numerical calculations based on the formalism of a modified eigenvalue formalism implemented with the axially symmetric FEM are also carried out to justify the previous analytical estimations without the substrate, confirm the resonance wavelengths, and obtain the field profiles [35]. The procedure has been conducted on a GaN nanoring cavity with satisfactory agreements [36]. In these calculations, the corrected refractive index of the ZnO microsphere obtained earlier is also adopted. With the schematic of a single ZnO microsphere on the Si substrate shown in Fig. 5(a), the field profiles of the WGM near the wavelength of 522.83 nm (l = 25) at D = 2.7 μm are numerically calculated and depicted in Fig. 5(b) for the top view on the equatorial plane, and in 5(c) for the side view on the vertical cross section. The mode number l is now half the number of bright spots along the azimuthal direction in Fig. 5(b). These field profiles confirm that the WGM is indeed confined near the equator and therefore less affected by the substrate. Due to the presence of the substrate which breaks the spherical symmetry, the modes in this micro-resonator cannot be rigorously classified as TE_r or TM_r modes. However, the WGMs with vertical field profiles close to that in Fig. 5(c) are expected to be similar to the true TE_r fundamental WGMs of the microsphere since the substrate effect is negligible for them. We therefore denote these modes as TE_r-like WGMs. On the other hand, if the diameter of the microsphere is close to or smaller than the wavelength (D<1 μm), these modes may be affected by the substrate and show quite low Q factors due to the significant radiative loss [48].

The resonance spectra obtained by FEM calculations for various TE_r-like WGMs are shown in Fig. 6(a). These sharp spectra indicate very high quality factors for these WGMs, which are not experimentally observed because ZnO may not be free from absorption, and the

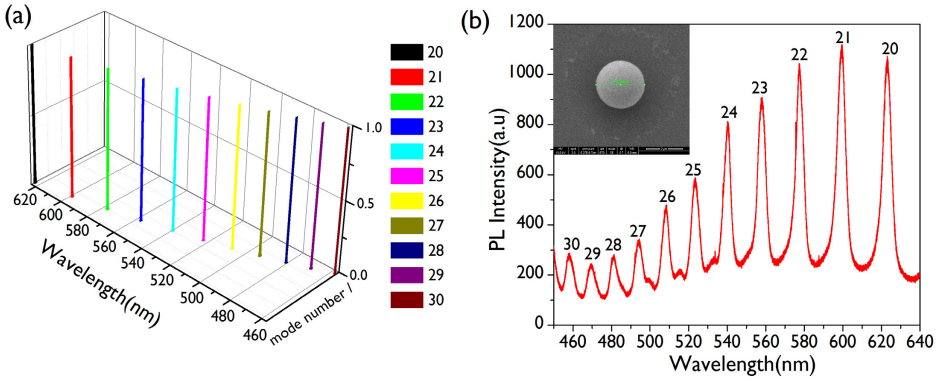

Fig. 6. (a) Resonances obtained from FEM calculations for different mode numbers l. The spectra are aimed at the TEr-like fundamental modes of the ZnO microsphere with D = 2.7 μm. (b) The mode assignments to the corresponding resonances on the PL spectrum.

#180785 - $15.00 USD Received 29 Nov 2012; revised 17 Jan 2013; accepted 22 Jan 2013; published 31 Jan 2013

microsphere is not perfectly smooth after all. On the other hand, the resonance wavelengths from FEM calculations agree well with the experimental data in Fig. 6(b), in which the mode numbers *l* are also assigned to the corresponding resonances. The values of resonance wavelengths obtained from FEM calculations are also listed in Table 1 for comparison.

5. Conclusions

In summary, we have presented a study on the cavity modes of single ZnO microspheres with smooth surfaces. ZnO microspheres prepared with the presented technique show good crystalline quality after annealing at high temperature. Prominent WGM resonances in microspheres can be observed in μ-PL measurements over the entire visible and partial near-IR windows. The comparison between the measured cavity resonances and theoretical calculations indicate the refractive index of ZnO microsphere is lower than that of bulk ZnO. The clear and narrow resonance peaks of these ZnO microspheres make them a promising candidate in the applications of future optoelectronic devices and developments of WGM-based biosensors.

Acknowledgments

This work is supported by Academia Sinica, Taiwan and National Science Council (NSC), Taiwan, under contracts NSC-101-2112-M-001-024-MY3 and NSC-100-2112-M-001-002-MY2.

#180785 - $15.00 USD Received 29 Nov 2012; revised 17 Jan 2013; accepted 22 Jan 2013; published 31 Jan 2013